Perfect Absorption in a Disordered Medium with Programmable Meta-Atom Inclusions

Mohammadreza F. Imani, David R Smith, Philipp del Hougne

Perfect Absorption in a Disordered Medium with Programmable Meta-Atom Inclusions

Mohammadreza F. Imani, David R. Smith, and Philipp del Hougne*

Dr. Mohammadreza F. Imani, Prof. David R. Smith,
Center for Metamaterials and Integrated Plasmonics
Department of Electrical and Computer Engineering
Duke University
Durham, NC 27708, USA

Dr. Philipp del Hougne
Institut d'Electronique et de Télécommunications de Rennes
CNRS UMR 6164
Université de Rennes 1
35000 Rennes, France
Email: philipp.delhougne@gmail.com

Keywords:
programmable metamaterial, disorder, perfect absorption, secure communication

Achieving the very special condition of perfect absorption (PA) in a complex scattering enclosure promises to enable a wealth of applications in secure communication, precision sensing, wireless power transfer, analog signal processing and random lasing. Consequently, a lot of recent research effort was dedicated to proposing wave-front shaping protocols to implement coherent PA in complex scattering environments with tunable localized absorption as well as a tunable excitation frequency. Here, the conceptually different route of solely tweaking the randomness of the complex scattering environment in order to achieve PA is proposed. An experimental proof-of-concept in the microwave domain is provided where the randomness of a three-dimensional chaotic cavity is tuned with programmable meta-atom inclusions. The achievability and extreme sensitivity of the PA condition are systematically investigated. The presented technique can impose a PA condition at over hundred distinct frequencies within a small frequency band, enabling the proposal and experimental demonstration of a concrete practical application: receiver-powered secure wireless communication in a complex scattering enclosure. The presented fundamentally new perspective on PA applies to all types of wave phenomena; the experimental results foreshadow the large potential of this novel tool for minute wave control in sensing, communication and energy transfer.

1. Introduction

Perfect absorption (PA) of waves only occurs under very special conditions. Usually, an impedance mismatch between two media causes a partial reflection of wave energy at the interface[1]. The PA condition requires vanishing outgoing fields which can be associated with a zero of the non-Hermitian scattering matrix on the real frequency axis[2]. Various research tracks have provided routes toward PA of single-channel monochromatic excitation with a carefully engineered structure, and some parts of the literature refer to this condition as "critical coupling". On the one hand, PA of incident plane waves has been demonstrated with Salisbury screens and metasurfaces[3–9]. On the other hand, PA of a guided mode via critical coupling to a single-mode resonator has been reported[10,11]. For critical coupling, the coupling rate of the excitation channel must equal the resonator's intrinsic decay rate. More recently, these ideas were generalized to multi-channel monochromatic excitations. In these cases, the coherence of the incident channels becomes crucial: PA only occurs if the impinging wave front is an eigenvector of the scattering matrix that is associated with a zero eigenvalue[12,13]. Various experimental demonstrations with very regularly shaped planar and guided-mode structures were reported[14–18]. The extreme sensitivity to changes in the excitation or absorbing system makes PA a fascinating topic for fundamental research and is at the heart of its technological relevance in wave filtering, sensing, communication, energy harvesting and thermal emission control[13].

All of the above-described approaches rely on a carefully engineered material to achieve PA. Yet, given the ubiquity of disordered matter presenting random scattering effects for all wave phenomena, achieving PA in a random medium would unlock a wealth of new applications. Although in principle no fundamental limit prevents this, in practice it appears extremely complicated to adjust excitation and decay rate of a randomly scattering medium. Very recently, coherent PA in random scattering media has been studied[19–21] and demonstrated in proof-of-principle experiments[22,23]. These experiments consider systems in which attenuation is dominated by a tunable local loss center; a wide parameter space of frequencies and loss values is then searched to identify a setting in which a zero of the scattering matrix lies on the real frequency axis.

Here, we propose a novel route to placing a scattering matrix zero of a random medium on the real frequency axis that solely relies on judiciously tweaking the medium's randomness. Thereby, our technique adjusts the coupling rate of the fixed excitation channel to the medium's modes. If losses are localized rather than global, our technique also enables adjustments of the medium's intrinsic decay rate by controlling the wave's exposure to loss centers. To demonstrate the feasibility of our concept, we consider a three-dimensional complex multi-mode scattering enclosure excited by a single guided mode in the microwave domain. The randomness of our medium, a chaotic cavity[24] with global rather than local absorption effects, is tuned with a programmable metasurface[25] that locally reconfigures the cavity's boundary conditions[26]. We thereby achieve PA without the need to control the amount of loss in the system, we can dynamically switch PA on and

off at multiple nearby frequencies, and (since our cavity is excited by a single channel) we avoid the technologically burdensome need to control the impinging wave's amplitude and phase. We systematically investigate the achievability and sensitivity of the PA condition with our technique. Then, for the first time, we demonstrate a practical application of PA in a complex scattering enclosure: we propose and implement a unique wireless communication protocol that is physically secure and receiver-powered. Our PA technique can also be implemented for any other type of wave phenomenon, for instance, using piezoelectric or acousto-optical modulators to tweak the randomness of a multimode fiber at optical frequencies[27,28].

2. Principle and Achievability of PA

The reflected power $\frac{P_{out}}{P_{in}}$ in a complex scattering enclosure such as a chaotic cavity is a statistically distributed quantity[29–31], such that sufficiently large changes of frequency or configuration can be interpreted as drawing a new value from the distribution. Thus, one may "accidentally" come across low reflectance values. The probability of "accidentally" finding an extreme value of this distribution, as is PA with zero rather than "low" reflectance, is incredibly low. In our complex scattering enclosure (an electrically large irregularly shaped metallic structure) depicted in **Figure 1**a, the probability to find $\frac{P_{out}}{P_{in}} \leq 2.5 \times 10^{-7}$ is 7.5×10^{-6}. It is hence clear that "accidentally" coming across a PA condition is virtually impossible in our system. To visualize the "achievability" of a given reflectance value, we consider the ensemble of all available spectral and configurational realizations of our system (3201 frequency points, 2^{16} metasurface configurations). Based on the corresponding reflectance values, we plot the experimentally determined cumulative distribution function (CDF) $\Phi(\frac{P_{out}}{P_{in}})$ for our system in Figure 1d (blue line). 2.5×10^{-7} is the lowest reflectance we can measure directly due to the presence of measurement noise.

At the core of our technique is the idea to drastically increase the probability of finding a PA condition by judiciously tweaking the randomness of the complex scattering enclosure. Our system is equipped with a 4x4 1-bit-programmable metasurface, as shown in Figure 1a. As detailed in the Experimental Section and Supplementary Note 1, each programmable meta-atom has two digitalized states, i.e., "0" and "1", corresponding to two opposite electromagnetic (EM) responses. Although the detailed EM response characteristics of the two states are irrelevant for our scheme as long as they are distinct, the idea behind our metasurface design is to emulate Dirichlet or Neuman boundary conditions via a phase difference of roughly π.[32,33] With our 16 reconfigurable meta-atoms placed inside the chaotic cavity, we can thus tweak the chaotic cavity's randomness in 2^{16} distinct ways. For a given target frequency f_0, we optimize the metasurface configuration in order to minimize the reflected power at f_0. An example is shown for $f_0 = 20.18\ \mathrm{GHz}$ in Figure 1b. For reference, besides the optimal PA configuration, the

reflected power spectrum for two random configurations of the metasurface is shown. While the PA configuration achieves $\frac{P_{out}}{P_{in}} = 2.28 \times 10^{-7}$, the reflected power is on the order of 6×10^{-2} for the two random configurations. For the PA configuration, the corresponding trajectory of the frequency-dependent complex-valued reflection coefficient S_{11} in the Argand diagram crosses the origin at f_0; for the random configurations, the trajectory does not get close to the origin.

Based on an evaluation of the lowest achievable reflectance at each of the 3201 considered frequency points in the $19 - 24$ GHz band, we evaluate the CDF of the lowest achievable $\frac{P_{out}}{P_{in}}$ values in our metasurface-programmable system. The corresponding curve (red line) in Figure 1d shows that the tuning mechanism drastically improves the probability to find $\frac{P_{out}}{P_{in}} \leq 2.5 \times 10^{-7}$ by four orders of magnitude from 7.5×10^{-6} to 5.3×10^{-2}. With our metasurface-programmable system, the probability of finding a PA condition is thus tangible and indeed we encounter more than 100 frequencies at which PA is achievable within the considered frequency band. The area between the red and the blue curves in Figure 1d testifies to the substantial change of the CDF that we achieve.

In Figure 1e we take a closer look at the cloud of accessible S_{11} values in the Argand diagram for three representative frequencies. Ideally, such as in the first case, the cloud is centered on the origin. If the cloud only touches the origin as in the second case, the number of configurations yielding an S_{11} close to the origin is much smaller. In the third case, if the cloud is far from the origin, achieving PA is impossible. Several factors may contribute to the fact that in our system we cannot achieve PA at every desired frequency. On the one hand, the meta-atoms' frequency response is not flat and at certain frequencies their impact on the field is weaker, implying less control to tune the scattering matrix. On the other hand, the number of zeros in the vicinity of a desired frequency is very likely not constant for all considered frequencies. Both factors can contribute to an inability to place one of the scattering matrix zeros at the desired frequency on the real frequency axis.

Several possibilities to further enhance the achievability of PA clearly emerge. First, multi-bit-programmable meta-atoms would allow us to navigate a given S_{11} dot in the Argand diagram to place it exactly on the origin, at least for all target frequencies for which the origin is covered by the cloud. The tunability mechanism of our meta-atoms being a varactor rather than a PIN diode, in principle it would only take a more elaborate biasing circuitry to enable continuous control of the EM response of each meta-atom. We therefore faithfully expect that continuous tuning of the meta-atoms would enable a further significant improvement of the CDF. Only in cases like the third in Figure 1e PA would likely continue to be inaccessible despite multi-bit programmability. This issue could be resolved by using more programmable meta-atoms which would increase the radius of the clouds. In Figure 1d we illustrate the reverse effect, namely of using fewer meta-atoms, on

the PA achievability. With 8 instead of 16 1-bit programmable meta-atoms, the probability of $\frac{P_{out}}{P_{in}} \leq 2.5 \times 10^{-7}$ drops from 5.3×10^{-2} to 7.0×10^{-4} but still remains significantly above that of 2.5×10^{-7} if the randomness is not tuned. For the cases of using only 4 or 2 programmable meta-atoms, it is evident in Figure 1d that the CDF curves are not smooth at low values of $\frac{P_{out}}{P_{in}}$ which indicates insufficient statistics (despite having run 45,000 realizations). Having outlined a clear route toward achieving PA at virtually any desired frequency, we point out that in fact achieving PA at a few frequencies as in our experiment is largely sufficient for many applications. Moreover, it is worthwhile acknowledging that wave-front-shaping-based coherent PA schemes as proposed in Refs.[22,23] rely on the frequency as free parameter to find a coherent PA condition, that is, by construction these methods are unable to achieve PA at any desired target frequency.

The impact of the complex scattering enclosure's Q-factor on the achievability of the PA condition is of practical importance to clarify whether our technique can be applied to a variety of settings. It is also of fundamental interest to understand if our technique can balance the coupling rate of the excitation channel with different values of the system's intrinsic decay rate. To lower the system's Q-factor, we add slots to the wall opposite the metasurface (see Figure S3 and Supplementary Note 4). The more slots there are and the larger they are, the more energy leaks out of the cavity, resulting in a lower Q-factor. In **Figure 2** we plot the CDF of $\frac{P_{out}}{P_{in}}$ for using a random and for using the optimal configuration of the metasurface, for three different Q-factors. First, we observe that PA is achievable irrespective of the Q-factor in our system. Second, the CDF for the random system does not significantly depend on the Q-factor. Third, the CDF of the tailored random system deteriorates slightly as the Q-factor decreases. At first sight, this may appear counterintuitive: a system with more loss is worse at perfectly absorbing a wave. However, achieving PA does not rely on maximizing attenuation in the system but on balancing excitation and attenuation rate. As evidenced in Supplementary Note 4, the control over the wave field needed to this end increases with the Q-factor.

3. Sensitivity

The very narrow reflectance dip in Figure 1b already hints at the extreme sensitivity of the PA condition. Since this sensitivity is crucial for the concept's technological relevance, here we systematically study the impact of geometry and frequency detuning on the PA condition. A convenient way to implement geometry detuning in our setup is to tune the configuration of one meta-atom away from that imposed by the optimal metasurface configuration. Given the meta-atom's 1-bit-programmability in our setup, this geometric detuning is thus not continuous. For the 168 frequencies for which an optimal metasurface configuration achieves $\frac{P_{out}}{P_{in}} < 10^{-6}$ in our system, we measure the reflected power if one

meta-atom is detuned. The resulting change of $\frac{P_{out}}{P_{in}}$ on a logarithmic scale is shown in **Figure 3**a, and the probability density function (PDF) θ of this quantity is plotted in Figure 3b. Except for the first two meta-atoms, detuning a single meta-atom is seen to systematically increase the reflected power by 40 to 50 dB, such that the detuned system with $\frac{P_{out}}{P_{in}}$ on the order of 10^{-2} does not present PA anymore. The PDF for the first two meta-atoms has two peaks, one around 40 to 50 dB and one around 0 dB. In roughly half of the considered PA cases, detuning one of the first two meta-atoms does therefore not destroy PA. Although the first two meta-atoms are the most distant ones from the port, since the other meta-atoms do not display any similar effect, we speculate that this effect must be an artefact due to some technical defect (see Supplementary Note 2).

To investigate frequency detuning, first, we interpolate our measured reflection spectra. While interpolating the reflection magnitude is not possible due to its rapid variation (the narrowness of the dip), real and imaginary part of S_{11} vary much slower (see Figure 1c) such that they can be interpolated faithfully. In Figure 3c we plot the change of $\frac{P_{out}}{P_{in}}$ on a logarithmic scale as the frequency is tuned above or below f_0. Occasionally, for very small detuning strengths, the reflected power decreases at first in one direction, as for the green line in the inset of Figure 3c. Due to the relatively coarse frequency sampling of our initial measurement, in these cases f_0 did not correspond precisely to the reflection dip's minimum. The high sensitivity of PA to frequency detuning is evidenced by the PDF of the change of $\frac{P_{out}}{P_{in}}$ on a logarithmic scale in Figure 3d. Upon detuning the frequency by a few MHz, the reflected power increases by 50 dB on average such that the PA condition is destroyed. The frequency detuning strength needed to destroy PA is thus at least an order of magnitude below the spectrum's characteristic correlation frequency f_0/Q (see Experimental Section) and at least four orders of magnitude smaller than f_0. Although for a given PA condition the reflection dip is not symmetrical for frequencies below and above f_0, the PDF is symmetrical.

We have studied two important sensitivities of PA related to geometry and frequency detuning. We faithfully expect that further extreme sensitivities exist, e.g. with respect to the spatial position of the port. An experimental investigation thereof is impossible since moving the port would simultaneously distort the geometry of our three-dimensional system. Nonetheless, since space and time tend to display analogous behavior in complex scattering environments, for instance, with respect to focusing[34], a very high sensitivity to spatial detuning is likely. Preliminary numerical results also point in that direction, as does Ref.[22] for wave-front-shaping based coherent PA.

4. Receiver-Powered Secure Wireless Communication

We now propose and demonstrate a concrete practical application of our PA technique which leverages the two above-established features of (i) extreme sensitivity and (ii) achievability at many distinct nearby frequencies. The security of wireless communication is a major concern in many areas and to date most security features are software-based, i.e. using some sort of encryption of the transferred data. Here, we propose and demonstrate how the extreme sensitivity of the PA condition can be leveraged to implement secure communication on the hardware level, without any need for data encryption. A further striking feature of our proposed communication system is that it is receiver-powered such that the transmitter can transfer information at high security without any noteworthy power consumption. To establish a wireless communication channel between Alice and Bob, conventionally, Alice actively emits electromagnetic waves that are received by Bob. With the advent of programmable metasurfaces, engineering the communication channels by tuning the propagation environment has become conceivable[35,36]. However, programmable metasurfaces can also be used to imagine novel backscatter-communication concepts for information transfer that do not rely on an active generation of waves by Alice. For instance, Alice can instead communicate with Bob by using a programmable metasurface to focus already existing stray ambient waves on Bob's receiver.[37] Here, we propose a scheme whereby Alice configures the propagation environment to switch PA on and off at Bob's port. One potential area for deployment is future radiofrequency-based chip-to-chip communication[38] where the propagation channels are known to be static[39].

If an eavesdropper Eve appears once the communication between Alice and Bob has been established, Eve's presence will detune the geometry and destroy PA, revealing her presence. Thus communication between Alice and Bob can only take place if its physical security is guaranteed. We can thus focus on the case of Eve being part of the communication system since the beginning. If Alice alternates between the special PA configuration and a random one, or between two PA configurations for two distinct frequencies, she can emulate amplitude-shift keying or frequency-shift keying protocols. Although PA is only observable on Bob's port, with a high dynamic range Eve could detect the switching between two fixed configurations and decode the binary message up to a confusion regarding which configuration is "0" and which is "1". Since, however, we can easily achieve PA at several frequencies, "1" (resp. "0") can be defined as creating a PA (resp. nonPA) condition for Bob's port at a randomly chosen frequency. In **Figure 4**a, we show a selection of eight PA and eight nonPA configurations for our modified experimental setup including a second eavesdropper port as depicted in Figure 4b. Note that the ability to achieve eight PA configurations within a 0.04 GHz bandwidth, as well as the ability to dynamically switch between PA and nonPA at each of these nearby frequencies, is a unique feature of our PA technique based on tuned randomness, setting it clearly apart from previous reports on PA in random media[22,23] (see also Discussion below). As illustrated in Figure 4c, for each bit, Alice randomly picks one of the eight configurations that yield

PA (resp. nonPA) at Bob's port in order to send a "1" (resp. "0").

To eavesdrop on the communication, Eve could attempt to measure the field emitted by Bob as Bob measures his port's reflectance. However, even in the best-case scenario for Eve, if Bob uses the same incident field throughout, the transmission from Bob to Eve does not appear to carry any useful information upon visual inspection (see Figure 4c). If Eve is less careful about being detected, she could also monitor the reflectance on her own port but again, this signal does not appear to carry any useful information (see Figure 4c). To further confirm that Eve cannot receive any useful information, we trained a custom self-supervised artificial neural network (ANN) since Eve does not have access to a labelled data set. As detailed in Supplementary Note 8, our autoencoder essentially compresses each measurement into a two-dimensional hidden space which can be visualized for subsequent cluster analysis. While PA and nonPA configurations can be clearly distinguished based on Bob's reflection measurement, neither the transmission from Bob to Eve nor Eve's reflection measurement enable an identification of PA/nonPA clusters. Our analysis in Figure 4c therefore demonstrates that our proposed communication scheme flawlessly transfers information from Alice to Bob at high security: Bob correctly receives all bits and Eve cannot extract any information about what bits Alice sends to Bob. In both cases, Eve will only observe a series of random signals irrespective of her dynamic range. Bob could add a further level of security by varying the incident field he uses over time. Finally, imagine the presence of a manipulator Mike, also equipped with a programmable metasurface. Mike could not pretend to be Alice and impose PA on Bob's port without Alice's collaboration.

5. Discussion

The extremely narrow reflection dip associated with the PA condition, as seen in Figure 1b, makes our experimental setup very attractive for wave filtering applications. High-quality filters are often based on copper cavities with very high Q-factors that must be tuned painstakingly by hand. In contrast, our complex scattering enclosure is made from simple copper tape and its average Q-factor is only on the order of 10^3 (see Experimental Section). Nonetheless, the PA condition may alter the resonance width distribution[40,41] and imposes an extremely narrow linewidth on the reflection spectrum at the PA condition. In Supplementary Note 5, we outline further potential applications of our PA technique to nondestructive high-precision evaluation and long-range efficient energy transfer.

Our technique of tuning the medium's randomness to achieve PA can be generalized to multiple excitation channels in different ways. One possibility is to engineer the disorder such that one eigenvalue of the scattering matrix is zero at a desired frequency, enabling coherent PA by using the corresponding eigenvector as impinging wave front. The difficulty of achieving (coherent) PA does not directly depend on the number of channels but is related to the challenge of moving *one* scattering matrix zero onto the real frequency axis. To circumvent the need for individual phase and amplitude control on each channel, one may impose as additional constraint that the CPA state should correspond to a

predefined vector. In either case the strict coherence requirement means that tiny events perturbing the channels outside the random system may result in an undesired vulnerability. Alternatively, one could attempt to force all scattering matrix entries to zero such that the outgoing field vanishes for any impinging wave front. If the scattering matrix has multiple zero eigenvalues, this will result in degenerate coherent-PA modes[2,42]. The technological burden of achieving PA in a random medium excited by multiple channels is inevitably larger than in the case of single-channel excitation. Yet, the use of multi-channel excitation would not improve the promises held by any of the discussed applications such that the use of single-channel excitation as in our experiments appears more enticing.

We now comment on a few advantages of our method to tune the random medium's disorder over the methods reported in Refs.[22,23] which rely on the operation frequency being a free parameter, the availability of coherent control of the impinging wave front and the freedom to tune the random medium's level of attenuation. Naturally, since we consider single-channel excitation as justified above, the simplicity of our setup (Arduino microcontroller and printed-circuit-board metasurface) is in sharp contrast to the immense hardware cost entailed by the need for precise amplitude and phase tuning of the incident wave front, e.g. with 16 IQ-modulators in Ref.[22]. Beyond this obvious advantage, from an experimental point of view, our technique removes the need for *in situ* control of the system's attenuation (typically via a single tunable loss center). Moreover, many realistic scattering systems like our 3D enclosure present significant homogeneous attenuation which prevents full *in situ* control of attenuation with a single loss center as in Refs.[22,23]. Our proposal's ease of implementation (low hardware complexity and cost, no need to tune attenuation) will be a key enabler for the proliferation of PA-based applications in real life. Second, from a statistical point of view, since our technique allows us to access over 160 instances of PA conditions within the considered frequency band (and potentially significantly more with multi-bit programmable meta-atoms), we were able to study statistical properties such as $\Phi(\frac{P_{out}}{P_{in}})$ and $\theta(\Delta\frac{P_{out}}{P_{in}}\ [\mathrm{dB}])$. In contrast to the schemes from Refs. [22,23] where the frequency is needed as free parameter such that only a single PA condition (within a rather large frequency interval) is identified, our approach thus enables a fuller study of PA in connection with its statistical characteristics. Our technique's unique ability to achieve PA conditions at multiple nearby frequencies also underpins our proposed protocol for secure communication.

One may also wonder if our work could straight-forwardly be extended to achieving the opposite of PA, namely perfect reflection at the interface. However, since homogeneous absorption in the scattering enclosure inevitably entails some loss that cannot be avoided by the waves, the reverberating waves incident on the port will never be able to create a perfect destructive interference with the waves leaving the port – unless gain-programmable meta-atom[43] inclusions are used[44]. Perfect reflection may have technological relevance, for instance, to prevent an intruder's mobile device from emitting any waves and hence from communicating. Moreover, the perfectly reflected channel would act like an electromagnetic sink[45] with interesting sub-diffraction features.

6. Conclusion

To summarize, we proposed and demonstrated that solely tuning a random medium's disorder can constitute a route to achieving the very special condition of PA (also known as "critical coupling") for which a scattering matrix zero must be placed on the real frequency axis. In our experiment which leverages a programmable metasurface to tune a complex scattering enclosure, we thoroughly investigated the achievability of PA with our approach as well as the extreme sensitivity of PA to geometry or frequency detuning. Building on these results, we went on to propose and demonstrate a protocol for receiver-powered secure wireless communication. We expect our technique to impact many areas in need of minute wave control at microwave frequencies as well as for other wave phenomena.

7. Experimental Section

Design of programmable metasurface. The programmable metasurface is an ultrathin planar array of electronically reprogrammable meta-atoms. Programmable metasurfaces are a promising young member of the metamaterial family thanks to the ease of fabrication and their unique capability to manipulate electromagnetic fields in a reprogrammable manner. The designed programmable metasurface in our experiment consists of a 4x4 array of meta-atoms operating in the K-band around 21 GHz. The metasurface is based on Rogers 4003C substrate (1.5 mm thick, dielectric constant of 3.55 and loss tangent of 0.0027). Each meta-atom consists of a mushroom structure including a varactor (MACOM MAVR-011020-1411) which endows it with programmability. The detailed mushroom structure can be found in Supplementary Note 1. In our design, the metasurface is equipped with two shift registers and reprogrammed via an Arduino microcontroller. Although our varactor-based design in principle enables gray-scale tuning, our control circuitry restricts us to binary control (on/off). The two states of each meta-atom emulate perfect-electric-conductor and perfect-magnetic-conductor-like behavior at the center of the operation band, i.e. their response has a phase difference of roughly π. Note that the specific details of the meta-atom response are not important in our work; what matters is that reconfiguring the meta-atom has a notable impact on the cavity wave field. Further details on the metasurface are provided in Supplementary Note 1.

Proof-of-principle system. The complex scattering environment in our experiment is a chaotic cavity[24] of dimensions 11×11×5.5 cm^3 with a quality factor of $Q = 1063$. The reflection spectrum's average correlation frequency is thus $\Delta f_{corr} = \frac{f_0}{Q} \approx 20$ MHz. One corner is deformed into a sphere octant to introduce wave chaos. Electrically large cavities of irregular shape are termed "wave-chaotic" since the separation of two rays launched from the same location in slightly different directions increases exponentially in time. A 8×8 cm^2 area on one cavity wall is equipped with our home-made 4x4 programmable

metasurface. A WR42 rectangular waveguide is used to pump electromagnetic energy into the cavity. A 1m-long 50-Ω coaxial cable connects the WR42 waveguide port to the VNA in order to measure the frequency-dependent reflection coefficient (S_{11}). To keep the measurement noise low, we set the VNA's intermediate-frequency bandwidth to 5 kHz and work with a power of 0 dBm. The wall opposite to the programmable metasurface can be perforated with holes to introduce additional loss channels in a controlled manner. Further details on the experimental setup are provided in Supplementary Note 2.

Optimal metasurface configuration. Since there is no analytical forward model to predict the reflection spectrum as a function of the metasurface configuration, identifying the optimal configuration to approach PA as closely as possible at a desired target frequency is not straightforward. Most reports in the literature on tuning the randomness of a complex medium in other contexts relied therefore on lengthy sequential iterative trial-and-error methods implemented experimentally[26,35]. In certain practical applications in which only one PA configuration is needed, e.g. for precision sensing, an iterative optimization may be the best choice. However, such iterative solvers are not guaranteed to identify the globally optimal configuration. The immense experimental cost entailed by iterative optimizations precludes a statistical analysis of the PA condition as presented in our manuscript. Instead, we measure the reflection spectrum for all possible 2^{16} metasurface configurations, such that we can identify the globally optimal configuration at any desired frequency using any desired subset of meta-atoms.

Supporting Information

Supporting Information is available from the Wiley Online Library or from the author.

Acknowledgments

This work was supported in part by the Air Force Office of Scientific Research (AFOSR) (No. FA9550-18-1-0187). P.d.H. was supported in part by the French "Agence Nationale de la Recherche" under reference ANR-17-ASTR-0017.

Conflict of Interest

The authors declare no conflict of interest.

Author Contributions

P.d.H. conceived the idea, analyzed the data and wrote the paper. M.F.I. and P.d.H. conducted the experimental work. All authors contributed with thorough discussions and commented on the manuscript.

References

[1] D. M. Pozar, *Microwave Engineering*, John Wiley & Sons, **2009**.

[2] A. Krasnok, D. Baranov, H. Li, M.-A. Miri, F. Monticone, A. Alú, *Adv. Opt. Photon.* **2019**, *11*, 892.

[3] R. L. Fante, M. T. McCormack, *IEEE Trans. Antennas Propag.* **1988**, *36*, 1443.

[4] N. I. Landy, S. Sajuyigbe, J. J. Mock, D. R. Smith, W. J. Padilla, *Phys. Rev. Lett.* **2008**, *100*, 207402.

[5] X. Liu, T. Starr, A. F. Starr, W. J. Padilla, *Phys. Rev. Lett.* **2010**, *104*, 207403.

[6] Y. Yao, R. Shankar, M. A. Kats, Y. Song, J. Kong, M. Loncar, F. Capasso, *Nano Lett.* **2014**, *14*, 6526.

[7] W. Withayachumnankul, C. M. Shah, C. Fumeaux, B. S.-Y. Ung, W. J. Padilla, M. Bhaskaran, D. Abbott, S. Sriram, *ACS Photonics* **2014**, *1*, 625.

[8] V. S. Asadchy, I. A. Faniayeu, Y. Ra'di, S. A. Khakhomov, I. V. Semchenko, S. A. Tretyakov, *Phys. Rev. X* **2015**, *5*, 031005.

[9] C. M. Watts, X. Liu, W. J. Padilla, *Adv. Mater.* **2012**, *24*, OP98.

[10] M. Cai, O. Painter, K. J. Vahala, *Phys. Rev. Lett.* **2000**, *85*, 74.

[11] J. R. Tischler, M. S. Bradley, V. Bulović, *Opt. Lett.* **2006**, *31*, 2045.

[12] Y. D. Chong, L. Ge, H. Cao, A. D. Stone, *Phys. Rev. Lett.* **2010**, *105*, 053901.

[13] D. G. Baranov, A. Krasnok, T. Shegai, A. Alù, Y. Chong, *Nat. Rev. Mater.* **2017**, *2*, 17064.

[14] W. Wan, Y. Chong, L. Ge, H. Noh, A. D. Stone, H. Cao, *Science* **2011**, *331*, 889.

[15] J. Zhang, K. F. MacDonald, N. I. Zheludev, *Light Sci. Appl.* **2012**, *1*, e18.

[16] R. Bruck, O. L. Muskens, *Opt. Express* **2013**, *21*, 27652.

[17] S. M. Rao, J. J. Heitz, T. Roger, N. Westerberg, D. Faccio, *Opt. Lett.* **2014**, *39*, 5345.

[18] Z. J. Wong, Y.-L. Xu, J. Kim, K. O'Brien, Y. Wang, L. Feng, X. Zhang, *Nat. Photonics* **2016**, *10*, 796.

[19] Y. V. Fyodorov, S. Suwunnarat, T. Kottos, *J. Phys. A* **2017**, *50*, 30LT01.

[20] H. Li, S. Suwunnarat, R. Fleischmann, H. Schanz, T. Kottos, *Phys. Rev. Lett.* **2017**, *118*, 044101.

[21] H. Li, S. Suwunnarat, T. Kottos, *Phys. Rev. B* **2018**, *98*, 041107.

[22] K. Pichler, M. Kühmayer, J. Böhm, A. Brandstötter, P. Ambichl, U. Kuhl, S. Rotter, *Nature* **2019**, *567*, 351.

[23] L. Chen, T. Kottos, S. M. Anlage, *arXiv:2001.00956* **2020**.

[24] U. Kuhl, H.-J. Stöckmann, R. Weaver, *J. Phys. A: Math. Gen.* **2005**, *38*, 10433.

[25] T. J. Cui, M. Q. Qi, X. Wan, J. Zhao, Q. Cheng, *Light Sci. Appl.* **2014**, *3*, e218.

[26] M. Dupré, P. del Hougne, M. Fink, F. Lemoult, G. Lerosey, *Phys. Rev. Lett.* **2015**, *115*, 017701.

[27] S. Resisi, Y. Viernik, S. M. Popoff, Y. Bromberg, *APL Photonics* **2020**, *5*, 036103.

[28] M. Bello-Jiménez, E. Hernández-Escobar, A. Camarillo-Avilés, O. Pottiez, A. Díez, M. V. Andrés, *Laser Phys. Lett.* **2018**, *15*, 085113.

[29] R. A. Méndez-Sánchez, U. Kuhl, M. Barth, C. H. Lewenkopf, H.-J. Stöckmann, *Phys.*

Rev. Lett. **2003**, *91*, 174102.
[30] S. Hemmady, X. Zheng, E. Ott, T. M. Antonsen, S. M. Anlage, *Phys. Rev. Lett.* **2005**, *94*, 014102.
[31] X. Zheng, T. M. Antonsen, E. Ott, *Electromagnetics* **2006**, *26*, 3.
[32] D. Sievenpiper, J. Schaffner, R. Loo, G. Tangonan, S. Ontiveros, R. Harold, *IEEE Trans. Antennas Propag.* **2002**, *50*, 384.
[33] T. Sleasman, M. F. Imani, J. N. Gollub, D. R. Smith, *Phys. Rev. Applied* **2016**, *6*, 054019.
[34] F. Lemoult, G. Lerosey, J. de Rosny, M. Fink, *Phys. Rev. Lett.* **2009**, *103*, 173902.
[35] P. del Hougne, M. Fink, G. Lerosey, *Nat. Electron.* **2019**, *2*, 36.
[36] M. D. Renzo, M. Debbah, D.-T. Phan-Huy, A. Zappone, M.-S. Alouini, C. Yuen, V. Sciancalepore, G. C. Alexandropoulos, J. Hoydis, H. Gacanin, J. de Rosny, A. Bounceur, G. Lerosey, M. Fink, *J. Wireless Com. Network* **2019**, *2019*, 129.
[37] H. Zhao, Y. Shuang, M. Wei, T. J. Cui, P. del Hougne, L. Li, *Nat. Commun.* **2020**, in press, *arXiv:2001.09567*.
[38] M. F. Chang, V. P. Roychowdhury, L. Zhang, H. Shin, Y. Qian, *Proc. IEEE* **2001**, *89*, 456.
[39] X. Timoneda, S. Abadal, A. Franques, D. Manessis, J. Zhou, J. Torrellas, E. Alarcón, A. Cabellos-Aparicio, *IEEE Trans. Commun.* **2020**, *68*, 3247.
[40] E. Persson, I. Rotter, H.-J. Stöckmann, M. Barth, *Phys. Rev. Lett.* **2000**, *85*, 2478.
[41] U. Kuhl, R. Höhmann, J. Main, H.-J. Stöckmann, *Phys. Rev. Lett.* **2008**, *100*, 254101.
[42] J. R. Piper, V. Liu, S. Fan, *Appl. Phys. Lett.* **2014**, *104*, 251110.
[43] L. Chen, Q. Ma, H. B. Jing, H. Y. Cui, Y. Liu, T. J. Cui, *Phys. Rev. Applied* **2019**, *11*, 054051.
[44] E. Rivet, A. Brandstötter, K. G. Makris, H. Lissek, S. Rotter, R. Fleury, *Nat. Phys.* **2018**, *14*, 942.
[45] J. de Rosny, M. Fink, *Phys. Rev. Lett.* **2002**, *89*, 124301.

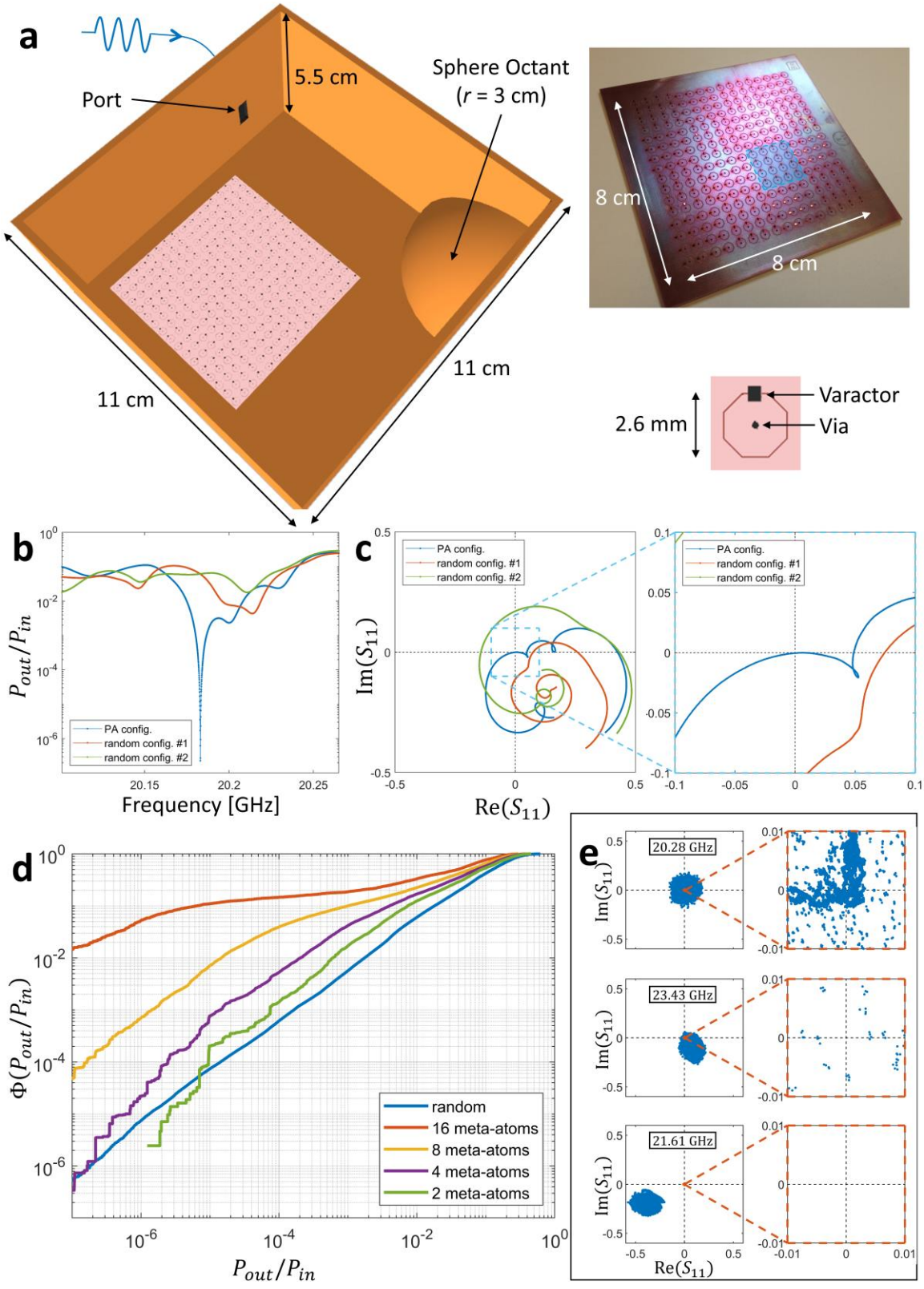

Figure 1. Experimental setup, PA principle and PA achievability. a, A monochromatic guided mode excites a complex scattering enclosure (top wall removed to show interior), including a sphere octant to perturb the otherwise regular cavity modes, and our 4x4 programmable metasurface.

One meta-atom is highlighted in the photographic image of the programmable metasurface. Each 1-bit-programmable meta-atom consists of 16 mushroom structures. Details of the latter are shown as inset. **b,** Experimentally measured reflected power for the PA metasurface configuration ($f_0 = 20.18$ GHz) as well as for two random metasurface configurations. **c,** Trajectories of the frequency-dependent complex-valued reflection coefficient S_{11} in the Argand diagram corresponding to the three curves in **b**. A zoom is provided as inset. **d,** Experimentally determined cumulative distribution function $\Phi(P_{out}/P_{in})$ of the reflected power for our complex scattering enclosure. The blue curve is based on the $19 - 24$ GHz band and all possible metasurface configurations. The remaining lines consider for each frequency point only the reflected power corresponding to the optimal metasurface configuration, for different numbers of programmable meta-atoms. **e,** Clouds of all accessible reflection coefficients with our 1-bit programmable metasurface in the Argand diagram for three selected frequencies. A zoom is provided as inset.

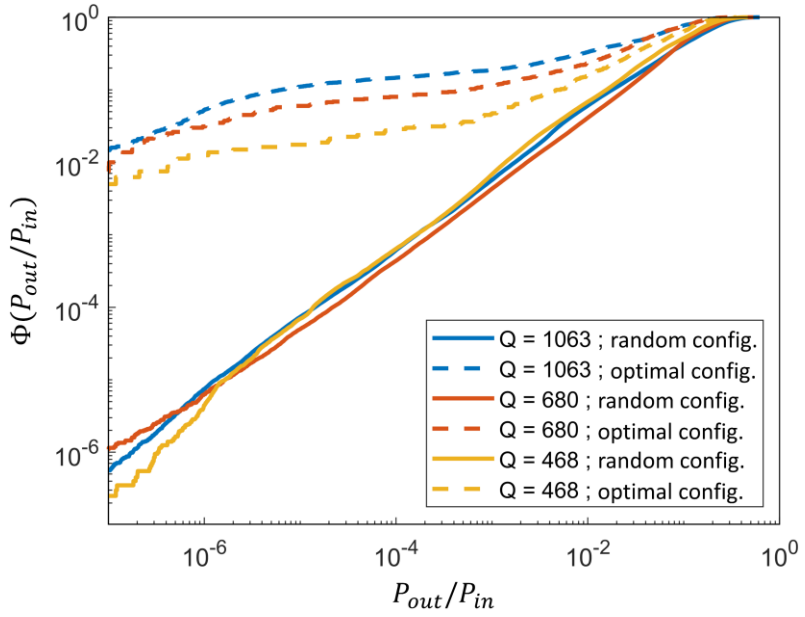

Figure 2. CDF of reflected power at various Q-factors. The experimentally determined cumulative distribution function $\Phi(P_{out}/P_{in})$ for complex scattering enclosures with three different Q-factors (color-coded, see legend) are shown. The continuous curves are based on the $19-24$ GHz band and all possible metasurface configurations. The dashed lines consider for each frequency point only the reflected power corresponding to the optimal metasurface configuration (using all 16 programmable meta-atoms).

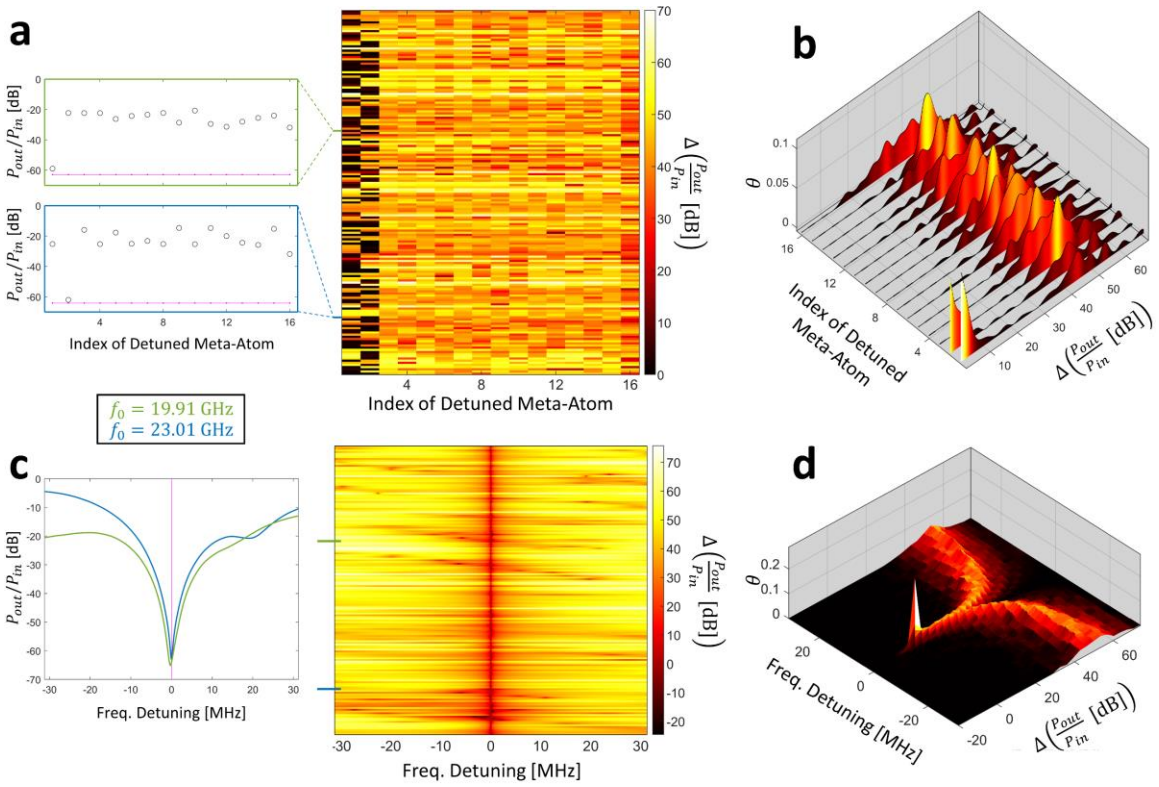

Figure 3. Sensitivity of PA condition to geometry and frequency detuning. a, Sensitivity to geometry detuning. The change of $\frac{P_{out}}{P_{in}}$ on a logarithmic scale upon flipping one meta-atom's configuration from "0" to "1" or vice versa is shown for 168 frequencies for which the optimal metasurface configuration achieves $\frac{P_{out}}{P_{in}} < 10^{-6}$. The inset shows for two representative frequencies the reflected power with the optimal metasurface configuration (purple line) as well as for the 16 configurations with one detuned meta-atom. **b,** For each meta-atom, the PDF θ of the change of $\frac{P_{out}}{P_{in}}$ on a logarithmic scale upon detuning is shown, evaluated based on the 168 frequencies considered in **a**. **c,** Sensitivity to frequency detuning. The change of $\frac{P_{out}}{P_{in}}$ on a logarithmic scale upon detuning the PA frequency f_0 is shown for 168 frequencies for which the optimal metasurface configuration achieves $\frac{P_{out}}{P_{in}} < 10^{-6}$. The inset presents the reflected power as function of the detuning frequency for two representative frequencies. **d,** For each considered frequency-detuning strength, the PDF θ of the change of $\frac{P_{out}}{P_{in}}$ on a logarithmic scale is shown, evaluated based on the 168 frequencies considered in **d**.

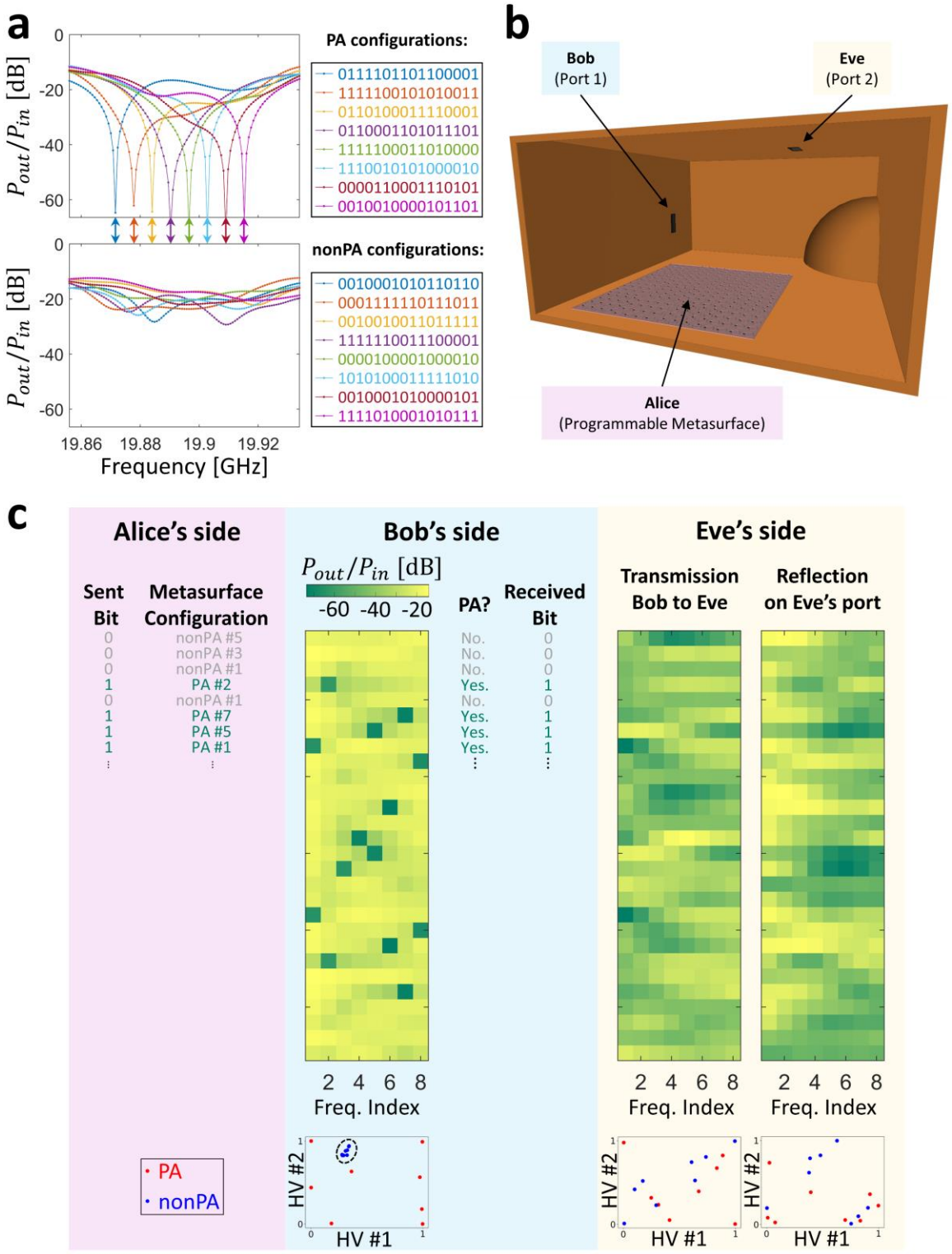

Figure 4. Receiver-powered secure wireless communication. **a,** Selection of eight metasurface configurations yielding PA at eight corresponding frequencies (indicated with arrows) as well as eight configurations not yielding PA at these frequencies. **b,** Experimental setup including a second (eavesdropper) port (front wall removed to show interior). **c,** *In situ* measurements of information transfer from Alice to Bob using randomly chosen PA (nonPA) configurations out of those

identified in **a** to encode “1” (“0”). Simultaneously, the signals that Eve can obtain by receiving the signals emitted by Bob or measuring her port’s reflectance are measured. To confirm that both are random and do not reveal what information Alice sends to Bob, a cluster analysis based on an ANN autoencoder is included as inset on the bottom (see Supplementary Note 8). While PA and nonPA configurations can clearly be clustered in the two-dimensional hidden variable (HV) space based on Bob’s reflection measurement, this is not the case for Eve’s measurements.

ToC:

By doping a disordered material with programmable meta-atom inclusions, its scattering properties can be tuned such that incident radiation is perfectly absorbed. The extreme sensitivity of this special perfect-absorption condition, as well as its broad achievability, are investigated and leveraged in a novel scheme for physically secure receiver-powered wireless communication.

M. F. Imani, D. R. Smith, P. del Hougne*

Perfect Absorption in a Disordered Medium with Programmable Meta-Atom Inclusions

ToC figure: